Wideband Large-Signal RF Measurements Applied to Behavioral Model Extraction

Maciej Myslinski[1], Dominique Schreurs[1], Kate A. Remley[2], Bart Nauwelaers[1]

[1]K.U.Leuven, Div. ESAT-TELEMIC, Kasteelpark Arenberg 10, B-3001 Leuven, Belgium
e-mail: maciej.myslinski@esat.kuleuven.be; phone: +32-16-321117; fax: +32-16-321986
[2]National Institute of Standards and Technology, Electromagnetics Division, 325 Broadway; Boulder, CO 80305, USA
e-mail: remley@boulder.nist.gov; phone: +1-303-497-3652, fax: +1-303-497-3970

***Abstract* — This paper presents, for the first time, wideband large signal network analyzer (LSNA) measurements used to extract a large-signal behavioral model of an RF amplifier. The methodology together with some important issues concerning the data processing are discussed. The procedure is illustrated by an example of a packaged buffer amplifier for wireless applications. We performed qualitative and quantitative analysis of the model's accuracy by means of wideband large-signal measurements and large-signal metrics, respectively. Additionally, we compare these results with those obtained from a behavioural model based on narrowband LSNA measurements.**

***Index terms* — Behavioral model, large-signal measurements, neural network applications, nonlinear systems, system analysis and design.**

I. INTRODUCTION

LSNA measurements have been used in prior work to extract accurate behavioral models of various RF devices and circuits for modern wireless communication systems [1, 2]. The LSNA set-up [3] measures the amplitude and phase of a discrete set of spectral components of the incident and scattered traveling voltage waves of the Device Under Test (DUT) excited with single-tone or band-pass multisine periodic signals. The latter excitations, when carefully chosen, can approximate complex digitally modulated signals omnipresent in modern telecommunication standards [4]. However, due to the frequency performance of the Analog to Digital Converters (ADC), commercially available LSNA set-ups are limited to a modulation bandwidth of 8 or 20 MHz, depending on the age of the unit. In practice, this value must be further decreased by a factor two or three, when we wish to assess nonlinear distortion. For example, in an adjacent channel power ratio (ACPR) calculation, all frequency components of interest must appear in the measurement bandwidth. This limitation on the modulation bandwidth is especially cumbersome when we consider that modern telecommunication applications involve modulation schemes with much larger bandwidths. An example of this is the 16.6 MHz bandwidth of an Orthogonal Frequency Division Multiplexing (OFDM) signal in the IEEE 802.11a™-1999 wireless local area network (WLAN) standard.

Recently, a measurement method has been proposed to increase the effective modulation bandwidth of the LSNA [5]. The main idea is to perform a series of measurements, each time setting the LSNA such that it covers overlapping frequency bands across the larger frequency band of interest. The final wideband LSNA data, calibrated in both magnitude and phase, are obtained in a post-processing procedure.

In this paper we present for the first time the large-signal time-domain behavioral model of an off-the-shelf RF amplifier extracted from wideband LSNA measurements. We discuss the modeling method and modifications to the measurement procedures of [5] required for modeling purposes. The ability of the derived model to predict the amplifier's behavior when it is excited by a 12 MHz multisine is verified by a 40 MHz band of LSNA measurements. The accuracy of the model's prediction is quantitatively analyzed and compared with the corresponding results obtained from a behavioral model extracted from narrowband LSNA measurements.

II. MODELING PROCEDURE

A. Model Description

The modeling method, based on [1], uses dynamic equations describing the behavior of a two-port RF component with no long-term memory in terms of traveling voltage waves:

$$b_1(t) = f_1(a_1(t), a_2(t), \dot{a}_1(t), \dot{a}_2(t), ..., \dot{b}_1(t), \dot{b}_2(t), ...), \quad (1)$$

$$b_2(t) = f_2(a_1(t), a_2(t), \dot{a}_1(t), \dot{a}_2(t), ..., \dot{b}_1(t), \dot{b}_2(t), ...). \quad (2)$$

In equations (1) and (2), $b_i(t)$ and $a_i(t)$ represent the scattered and the incident traveling voltage waves, respectively. The superscript dots denote time derivatives. The functional relationships $f_1(.)$ and $f_2(.)$ between the

minimal set of independent variables and the scattered traveling voltage waves are implemented by an Artificial Neural Network (ANN) with parameters found by optimization. The three-layer perceptron ANN is defined as:

$$\hat{b}_k(t) = y_k(t,x) = \sum_{i=1}^{m} w_{ki}^2 \sigma\left(\sum_{j=1}^{n} w_{ij}^1 x_j + s_i^1\right) + s_k^2 , \qquad (3)$$

where $k=1,2$ are the port numbers, n is the number of input neurons, equal to the number of independent variables, m is the number of hidden neurons, w^1_{ij} are the weights between the j^{th} neuron in the input layer and the i^{th} neuron in the hidden layer, s^1_i is the bias of the input layer, w^2_{ki} are the weights between the i^{th} neuron in hidden layer and the k^{th} neuron in output layer, s^2_k is the bias of the output layer, σ is the hidden layer neuron activation function, and x is the set of input independent variables.

The goal is to find the set of neural network parameters $\{\boldsymbol{w}^1, \boldsymbol{w}^2, \boldsymbol{s}^1, \boldsymbol{s}^2\}$ providing the lowest training and testing error during the ANN learning process. The unknown parameters are real numbers and time-independent.

B. Wideband Experiment Design

The accuracy and validity range of the large-signal time-domain behavioral model described in the previous section depend primarily on the experiment design. As highlighted in the Introduction, modern wireless telecommunication standards usually involve signals modulated in a bandwidth greater than that provided by the commercial LSNA set-up. Therefore the ability to extend the LSNA's effective modulation band and to measure the DUT's wideband behavior plays a key role in the construction of accurate large-signal models for current wireless telecommunication systems.

The wideband LSNA measurement method described in [5] provides the calibrated amplitude and phase information of the traveling voltage waves at the DUT ports in the desired modulation band. In order to achieve this, the desired bandwidth is divided into smaller overlapping sub-bands. It was shown in [5] that one has to provide at least two overlapping tones. The analysis in [5] was demonstrated for an IF spectrum around the RF carrier. However, for modeling purposes, the harmonic content is also of importance. When harmonics are included, this number of two has to be increased proportionally to the number of RF carrier harmonic components. This results from the frequency separation between the RF frequency harmonic grids of the measured adjacent sub-bands. As a result, the difference in frequency between the center frequencies of two adjacent sub-bands

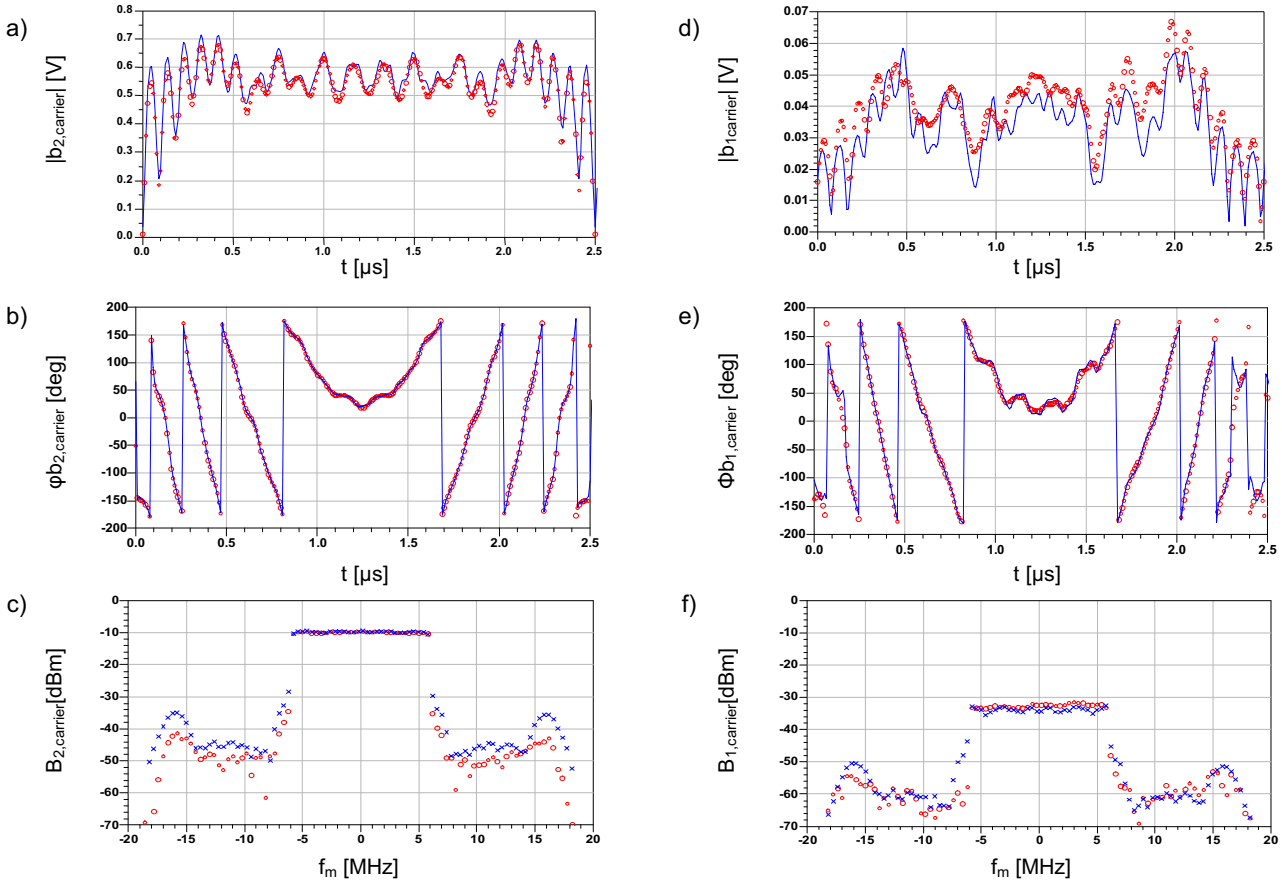

Fig. 1. The measured (blue line and x) and simulated (red circles): (a) magnitude waveform, (b) phase waveform, (c) amplitude spectrum of the complex envelope b_2 wave, and (d) magnitude waveform, (e) phase waveform, (f) amplitude spectrum of the complex envelope b_1 scattered traveling voltage wave around RF carrier frequency 4.9 GHz; the input power is 0 dBm.

increases proportionally to the RF harmonic index, while the measured modulation band remains constant regardless of the harmonic component considered.

IV. Results

A. Model Verification

The modeling approach presented was applied to an off-the-shelf general-purpose buffer RF amplifier developed for 4.9 GHz wireless applications. The circuit was measured under a 30-tone multisine excitation with a 12 MHz bandwidth centered at 4.9 GHz. The wideband large-signal data used to extract the model were acquired from the LSNA measurements in a 40 MHz band around the carrier frequency and up to its fourth harmonic. The desired band was divided into 19 overlapping sub-bands according to the procedure described in the previous section.

The model parameters were determined using the ANN training tool given in [6]. The training and testing data corresponded to the input power levels of +1 dBm and –1 dBm, respectively. The wideband data corresponding to the multisine at the input power of 0 dBm was used for the model simulation. The set of plots in Fig. 1 depicts both the time- and frequency-domain simulation results (red circles) together with the corresponding measurements (blue trace) of the b_2 and b_1 waves at port 2 and port 1, respectively. One can notice very good agreement between the measurements and the model predictions of the b_2 wave results. In case of the b_1 wave, the discrepancy between the measurements and simulations is relatively larger, but it occurs at a voltage level ten times lower than that for the b_2 wave.

In order to assess quantitatively the accuracy of the described model's prediction of the scattered traveling voltage waves b_1 and b_2, we will calculate the time-domain RMS error metric *TDRMS_Bk@harm* as in [7]:

$$\mathrm{TDRMS\_Bk@harm} = \sqrt{\frac{\sum_p \sum_n \left| b_{k,harm,sim}(n) - b_{k,harm,meas}(n) \right|^2}{\sum_p \sum_n \left| b_{k,harm,meas}(n) \right|^2}} \quad (4)$$

In equation (4), $b_{k,harm,sim}$ and $b_{k,harm,meas}$ represent the simulated and measured complex envelopes at port k and around *harm* (harmonic component of the carrier frequency), respectively. Indices n and p are the time sample index and the power level index, respectively.

The corresponding results are summarized in Table I. One can notice that the best prediction for the wideband model has been achieved for the b_2 scattered voltage wave at the carrier frequency. As expected, the corresponding b_1 wave at the carrier frequency is predicted with lower accuracy than that for the b_2 wave. In general, the RMS error for the port 1 output is higher than in the case of the corresponding wave at port 2. This might be due to the much lower signal level of the b_1 scattered traveling voltage wave, because the measured values are close to the noise floor of the test set-up. A similar explanation could be given for high RMS error value obtained for the b_2 wave measured at second and fourth harmonics.

B. Model Comparison

In previous work we showed that a large-signal behavioral model extracted from a multisine with a probability density function (PDF) corresponding to the statistical properties of a QPSK-modulated signal accurately predicts the behavior of an RF amplifier [7]. However the signals used for the model extraction and verification involved only typical LSNA measurements in an 8 MHz bandwidth around carrier frequency and its harmonics. It is interesting to see whether the behavioral model extracted and tested in the narrowband signal conditions can accurately predict the amplifier's response to the wideband excitation.

TABLE I. THE RESULTS OF THE ERROR METRIC (4) OBTAINED FOR THE WIDEBAND AND NARROWBAND MODELS SIMULATED WITH THE SAME COMPLEX ENVELOPES AROUND UP TO FOURTH RF HARMONIC.

Output wave / Metric	Wideband model		Narrowband model	
	b_1	b_2	b_1	b_2
TDRMS_B_k@f_0	0.246	0.055	2.244	0.649
TDRMS_B_k@$2f_0$	4.359	1.848	75.955	39.449
TDRMS_B_k@$3f_0$	1.959	0.375	1.901	2.325
TDRMS_B_k@$4f_0$	6.862	1.697	10.970	9.589

Therefore, we simulated the behavioral model that was extracted from a narrowband 63-tone multisine excitation having a 1.6 MHz bandwidth QPSK-shaped PDF, as described in [7]. However, we applied the same wideband signal conditions described in this work to the narrowband model. Fig. 2 presents the measured (blue crosses) and simulated (red circles) amplitude spectra of the complex envelope b_2 (a) and b_1 (b) scattered traveling voltage waves around the 4.9 GHz carrier frequency. By comparing these plots with similar graphs in Figs. 1 (c) and (f), one can notice a more significant discrepancy between measurements and simulations for the narrowband model. The main reason is that during the experiment the narrowband behavioral model is working outside its valid operational range. The extrapolation or interpolation of the operational range is usually very limited and leads to significant errors in prediction. This could also be the reason why the narrowband model's prediction is inaccurate even for frequencies close to the carrier frequency.

Following the qualitative analysis, a quantitative comparison of the prediction results obtained for both models is made. First of all, we calculate lower and upper ACPR by dividing the total power in the 12 MHz lower and upper adjacent channels by the total power in the main 12 MHz channel of the $B_{2,carrier}$ spectra. From the appropriate results summarized in Table II, one can see that both lower and upper

ACPR values are better predicted in the case of the wideband behavioral model. In the case of the narrowband model, the ACPR values are different by only up to 1 dB from those of the previous model, which seems rather small especially after comparing the plots of Fig. 2 (a). Due to its rational character, a constant shift in values is not included in the ACPR parameter.

TABLE II. THE RESULTS OF THE ACPR OBTAINED FOR THE WIDEBAND AND THE NARROWBAND MODELS SIMULATED WITH THE SAME COMPLEX ENVELOPES AROUND CARRIER FREQUENCY F_0=4.9 GHZ.

ACPR [dB]	Measured	Wideband model	Narrowband model
ACPR_lower	-15.072	-15.123	-14.795
ACPR_upper	-15.267	-15.087	-14.082

We observe similar results when the error metric (4) is calculated for the narrowband behavioral model and summarized in Table I. One can notice that, as with the wideband model, the narrowband model's prediction is most accurate for complex envelopes around the carrier and its third harmonic. However, even in these cases the accuracy is ten times worse than that for the wideband model.

All this confirms the need to extract the behavioral models directly from LSNA measurements with the same bandwidth as in the final application of the modeled circuit. In case of standards like IEEE802.11a, when the signal's bandwidth extends LSNA bandwidth, a special measurement method may be applied.

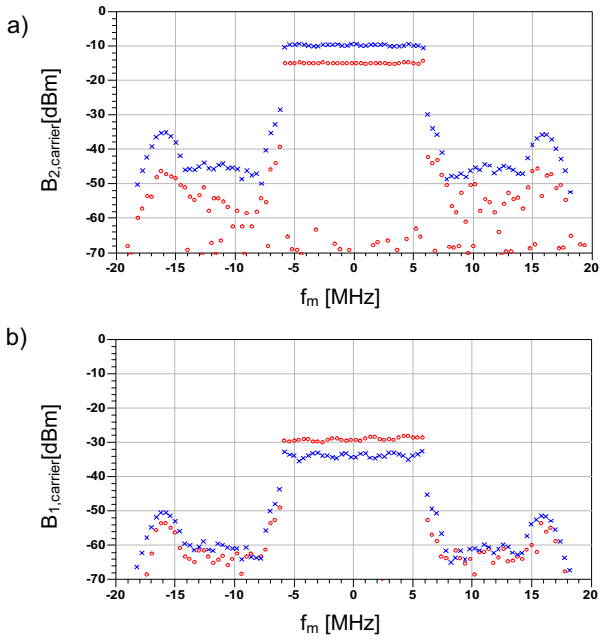

Fig. 2. The measured (blue x) and simulated (red circles) amplitude spectrum of the complex envelope (a) b_2, and (b) b_1 scattered traveling voltage wave around RF carrier frequency 4.9 GHz for the narrowband model; the input power is 0 dBm.

V. CONCLUSION

In this work, we have presented a method for applying wideband large-signal RF measurements to construct a large-signal behavioral model of an RF amplifier designed for modern wireless telecommunication applications. We described the modeling-related issues of the experiment design. The extracted model's prediction of the circuit's behavior in the modulation band around the carrier frequency was verified by both qualitative and quantitative analysis. Moreover, this modeling approach more accurately predicts an amplifier's response to a wideband excitation than does the behavioral model extracted from narrowband multisine LSNA measurements.

ACKNOWLEDGEMENT

Research reported here was performed in the context of the network TARGET– "Top Amplifier Research Groups in a European Team" and supported by the Information Society Technologies Programme of the EU under contract IST-1-507893-NOE, *www.target-net.org*. This work was partially funded by the FWO project G.0405.03. D. Schreurs is supported by the Fund for Scientific Research-Flanders as a postdoctoral fellow. Partial work of the U.S. government, not subject to copyright in the United States.

REFERENCES

[1] D. Schreurs, N. Tufillaro, J. Wood, D. Usikov, L. Barford, and D. E. Root, "Development of time domain behavioural non-linear models for microwave devices and ICs from vectorial large-signal measurements and simulations," *Proc. European Gallium Arsenide and related III-V compounds Applications Symposium*, Paris, France, pp. 236-239, 2-6 October 2000.

[2] J. Wood, "Nonlinear time series for black-box behavioral modeling of integrated circuits," *IEEE International Microwave Symposium (MTT-S) Workshop on WSG: Fundamentals of Nonlinear Behavioral Modeling: Foundations and Applications*, June 8, 2003.

[3] J. Verspecht, P. Debie, A. Barel, and L. Martens, "Accurate on wafer measurements of phase and amplitude of the spectral components of incident and scattered voltage waves at the signal ports of a nonlinear microwave device," *IEEE Digest of International Microwave Symposium (MTT-S)*, Orlando, USA, pp. 1029-1032, 16-20 May 1995.

[4] J.C. Pedro and N.B. Carvalho, "Designing multisine excitations for nonlinear model testing", *IEEE Transactions on Microwave Theory and Techniques*, Vol. 53, No. 1, pp. 45-54, Jan. 2005.

[5] K. A. Remley, D. Schreurs, and M. Myslinski, "Wideband Measurements of Phase Distortion With Narrowband Vector Receivers", submitted to *IEEE Transactions on Microwave Theory and Techniques*.

[6] Q. J. Zhang and K. C. Gupta, *Neural networks for RF and microwave design*, Artech House, 2000.

[7] M. Myslinski, D. Schreurs, K.A. Remley, M.D. McKinley and B. Nauwelaers, "Large-Signal Behavioral Model of a Packaged RF Amplifier Based on QPSK-Like Multisine Measurements", *Proc. Gallium Arsenide and other Compound Semiconductors Application Symposium (GAAS)*, Paris, France, pp. 185-188, 3-4 October 2005.